M.S. Thesis

Fast Terahertz Beam Management via Frequency-dependent Beamforming

주파수-종속 빔 형성 기반 빔 관리 기법 연구

BY

PARK JUNG-JAE

FEBRUARY 2023

DEPARTMENT OF ELECTRICAL ENGINEERING
AND COMPUTER SCIENCE
COLLEGE OF ENGINEERING
SEOUL NATIONAL UNIVERSITY

Fast Terahertz Beam Management via Frequency-dependent Beamforming

주파수-종속 빔 형성 기반 빔 관리 기법 연구

지도 교수 심 병 효
이 논문을 공학석사 학위논문으로 제출함

2023 년 2 월

서울대학교 대학원
전기정보공학부
박 정 재

박정재의 공학석사 학위논문을 인준함
2023 년 2 월

위 원 장	최 완	(인)
부위원장	심 병 효	(인)
위 원	이 경 한	(인)

Abstract

Terahertz (THz) communications are envisaged as an attractive way to attain richer spectrum resources and surmount the bandwidth desert. One main difficulty of the THz communication is the severe attenuation of signal power caused by the high diffraction and penetration losses and atmospheric absorption. To compensate for the severe path loss, a beamforming technique realized by the massive multiple-input multiple-output (MIMO) has been widely used. Since the beamforming gain is maximized only when the beams are appropriately aligned with the signal propagation paths, the acquisition of accurate beam directions is of great importance. A major issue of the conventional beam management schemes is the considerable latency being proportional to the number of training beams. In this paper, we propose a THz beam management technique that simultaneously generates multiple frequency-dependent beams using the true time delay (TTD)-based phase shifters. By closing the gap between the frequency-dependent beamforming vectors and the desired directional beamforming vectors using the TTD-based signal propagation network called intensifier, we generate very sharp training beams maximizing the beamforming gain. From the numerical results, we demonstrate that the proposed scheme achieves more than 70% reduction in the beam management latency and 60% increase in the data rate.

Keyword : Terahertz communications, massive MIMO, beam management
Student Number : 2021-26765

Contents

I. INTRODUCTION

Recently, terahertz (THz) communications have received much attention to alleviate spectrum bottleneck and support high data rates for 6G wireless communications [1], [2]. Using the abundant spectrum resource in the THz frequency band ($0.1 \sim 10$ THz), THz communications can support immersive mobile services such as digital twin, metaverse realized by XR devices, and high-fidelity mobile holographic displays [3], [4]. Well-known drawback of the THz communications is the severe attenuation of the signal power caused by the high diffraction and penetration losses and atmospheric absorption [5]. To deal with the problem, a beamforming technique realized by the massive multiple-input multiple-output (MIMO) has been widely used [6], [7]. Since the beamforming gain is maximized only when the beams are properly aligned with the signal propagation paths, the base station (BS) needs to acquire the accurate channel information in a form of angle-of-arrivals (AoAs) and angle-of-departures (AoDs). The process to acquire the AoAs/AoDs associated with the paths between the BS and the mobile and then send the directional beams to the acquired directions is collectively called *beam management* [8], [9]. In general, the beam management consists of two steps: 1) *beam sweeping* and 2) *beam refinement*. In the beam sweeping step, the BS sequentially transmits the training beams carrying the reference signal and the mobile reports the index of the beam corresponding to the highest reference signal received power (RSRP) to the BS. After that, in the beam refinement step, the BS narrows down the direction of the mobile by sending multiple pilot signals (e.g., channel state information reference signal (CSI-RS)) to the direction obtained from the beam sweeping [10].

Over the years, various beam management schemes have been proposed [11]–[14]. In [11], a beam management scheme using the hierarchical multi-level beam codebook has been proposed. In [12], [13], a beam management scheme that generates the training beam using the antenna deactivation technique has been proposed. In [14], a deep-learning (DL)-based beam selection technique for the mmWave communications has been proposed. In these schemes, the analog phase shifters are often used in the training beam generation to reduce the hardware cost and computational complexity. Since the analog phase shifters generate one training beam at a time, the BS can probe only one spatial direction in each time slot, incurring a considerable beam management latency being proportional to the number of training beams. Recently, to speed up the beam management process, multiple beam generation approaches have been proposed

[15], [16]. In these approaches, the true time delay (TTD)-based phase shifter, a unit generating a specific time delay using multiple switched delay lines, is employed for the training beam generation [17]. By controlling the propagation path of the RF transmission signals, a phase shift being proportional to the product of time delay and the signal frequency is induced to the RF signal. Since the BS can simultaneously generate multiple frequency-dependent training beams using the TTD-based phase shifters, the beam management latency can be reduced considerably. While this approach is promising, since micro-electromechanical systems (MEMS) relying on costly semiconductor lithographic process is used in switching the delay lines in the TTD, hardware complexity and implementation cost of the TTD are considerable[1] [18]. To reduce the hardware complexity and the implementation cost, a partially-connected structure where one TTD is connected to multiple antennas has been suggested [18]. While this so-called delay-phased precoding (DPP) scheme can save the hardware cost, it will cause a severe degradation of the beamforming gain due to the strong sidelobe power of the generated beams.

An aim of this paper is to put forth an efficient THz beam management technique reducing the beam management latency without the loss of beamforming gain. The proposed scheme, henceforth referred to as *frequency-dependent beamforming (FDB)*, simultaneously generates multiple frequency-dependent training beams using the TTD-based phase shifters. A distinctive feature of the FDB-based beam management over the previous efforts is that we exploit a deliberately designed TTD-based signal propagation network called *intensifier* to compensate for the difference between the desired beamforming vectors and the frequency-dependent beamforming vectors. Since the BS can search multiple directions simultaneously while suppressing the sidelobes of the beams, we can obtain the significant reduction in the beam management latency and at the same time achieve the maximum beamforming gain with very marginal increase in the number of TTDs.

From the beam misalignment probability analysis, we show that the probability of FDB to find out the optimal beam direction is much higher than that of DPP. Also, from the numerical evaluations on the realistic THz systems, we demonstrate that FDB significantly reduces the beam management latency over the conventional approaches. In particular, FDB achieves more than 90% reduction on the beam management latency over the conventional beam management scheme in 5G NR [19]. Even when compared with DPP, FDB achieves more than 70% beam

[1]The cost of the TTD is nearly 10 times higher than that of the analog phase shifter [17].

management latency reduction.

The rest of this paper is organized as follows. In Section II, we discuss the wideband THz system model. In Section III, we explain the FDB beam generation mechanism. In Section IV, we present the FDB-based beam management process and provide the beam misalignment analysis. In Section V, we present the simulation results and then conclude the paper in Section VI.

Notation: Lower and upper case symbols are used to denote vectors and matrices, respectively. The superscript $(\cdot)^{\mathrm{T}}$, $(\cdot)^{\mathrm{H}}$, and $(\cdot)^{\dagger}$ denote transpose, hermitian transpose, and pseudo-inverse, respectively. $\|\mathbf{x}\|$ is the Euclidean norm of a vector $\mathbf{x}$ and $\|\mathbf{X}\|_{\mathrm{F}}$ is the Frobenius norm of a matrix $\mathbf{X}$. $\mathrm{Re}\{x\}$ and $\mathrm{Im}\{x\}$ are the real and imaginary parts of x, respectively. $\mathbf{a}_N(x) = \left[1\, e^{jx} \cdots e^{j(N-1)x}\right]^{\mathrm{T}}$ is the $N \times 1$ array steering vector corresponding to x. Also, $\mathbf{X} \otimes \mathbf{Y}$ and $\mathbf{X} \odot \mathbf{Y}$ denote the Kronecker and Hadamard product of $\mathbf{X}$ and $\mathbf{Y}$, respectively.

II. Wideband Terahertz System

In this section, we briefly discuss the wideband THz MISO system model and true time delay, followed by a description of the conventional frequency-dependent beamforming technique.

A. Terahertz MISO-OFDM System Model

We consider a downlink THz MISO-OFDM system where a BS equipped with a uniform linear array (ULA) of N antennas serves a single-antenna mobile. The number of OFDM subcarriers is S, the carrier frequency is f_c, and the bandwidth is B. To reduce the hardware complexity, we consider the analog beamforming architecture where an RF chain is connected with N phase shifters[2]. Under this setup, the received signal y_i of the mobile at the i-th subcarrier is given by

$$y_i = \sqrt{P_t}\mathbf{h}_i^{\mathrm{H}}\mathbf{f}_i s_i + n_i, \quad i = 1, \cdots, S, \tag{1}$$

where P_t is the BS transmit power, $\mathbf{h}_i \in \mathbb{C}^N$ is the downlink THz channel vector from the BS to the mobile, $\mathbf{f}_i \in \mathbb{C}^N$ is the frequency-dependent beamforming vector, s_i is the transmit symbol, and $n_i \sim \mathcal{CN}(0, \sigma_n^2)$ is the Gaussian noise at the i-th subcarrier. The corresponding data rate R of the mobile is given by

$$R = \frac{1}{S}\sum_{i=1}^{S} \log_2\left(1 + \frac{P_t|\mathbf{h}_i^{\mathrm{H}}\mathbf{f}_i|^2}{\sigma_n^2}\right). \tag{2}$$

[2]The proposed scheme can be readily extended to the hybrid beamforming architecture scenario where multiple RF chains are connected to the phase shifters. In fact, when the number of RF chains is larger than one, one can generate the oversampled FDB beams between the FDB beams generated by the single RF chain.

As for the channel model, we use the frequency-selective line-of-sight (LoS)-based THz channel model where the downlink i-th subcarrier channel vector $\mathbf{h}_i \in \mathbb{C}^N$ from the BS to the mobile is expressed as [20]

$$\mathbf{h}_i = \sqrt{\rho}\alpha_i e^{-j2\pi f_i \tau}\mathbf{a}_N(\phi_i), \quad i = 1, \cdots, S, \tag{3}$$

where ρ is the large-scale fading coefficient accounting for the path loss and the shadow fading, $\alpha_i \sim \mathcal{CN}(0,1)$ is the small-scale fading coefficient, τ is the propagation delay, $f_i = f_c - \frac{B}{2} + \frac{B}{S-1}(i-1)$ is the i-th subcarrier frequency, and ϕ_i is the subcarrier channel direction at the i-th subcarrier, defined as[3]

$$\phi_i = \frac{f_i}{f_c}\pi \sin\varphi, \quad i = 1, \cdots, S, \tag{4}$$

where φ is the AoD at the BS. Also, $\mathbf{a}_N(\phi_i) \in \mathbb{C}^N$ is the array steering vector of BS given by

$$\mathbf{a}_N(\phi_i) = \left[1\, e^{j\phi_i} \cdots e^{j(N-1)\phi_i}\right]^{\mathrm{T}}. \tag{5}$$

From (2) and (3), one can easily see that the optimal beamforming vector $\mathbf{f}_i^*$ maximizing the achievable rate is $\mathbf{f}_i^* = \mathbf{a}_N(\phi_i)$. It is worth mentioning that the optimal beamforming vector for each subcarrier is different. In order to find out $\{\mathbf{f}_i^*\}_{i=1}^S$, one should acquire the channel directions $\{\phi_i\}_{i=1}^S$ for all subcarriers, which requires quite a bit of time.

B. True Time Delay-based Phase Shifter

In 5G NR, analog phase shifters are employed for the training beam generation. Since the generated phase is invariant to the frequency, beams for all subcarriers are directed toward the same spatial direction. Due to this limitation, analog phase shifters can generate only one training beam at a time and thus the beam management latency is directly proportional to the number of training beams [10]. In fact, the time to complete the beam management process of 5G can easily exceed 20 ms, making it difficult to support even a mild mobility of human's movement (e.g., walking).

Recently, approaches to generate multiple frequency-dependent beams using the TTD-based phase shifters have been proposed [15], [16]. Essence of these approaches is to exploit TTD,

[3]In the conventional mmWave systems, the difference between f_c and f_i is relatively small, and thus one can readily assume that $\gamma_i = \frac{f_i}{f_c} \approx 1$. This means that all subcarrier channel directions are almost identical. In the THz systems, however, the difference between f_c and f_i is no longer negligible due to the large bandwidth. Thus, γ_i can be larger or smaller than 1. This phenomenon where the subcarrier channel direction depends on the subcarrier frequency is called the *beam squint effect* [21].

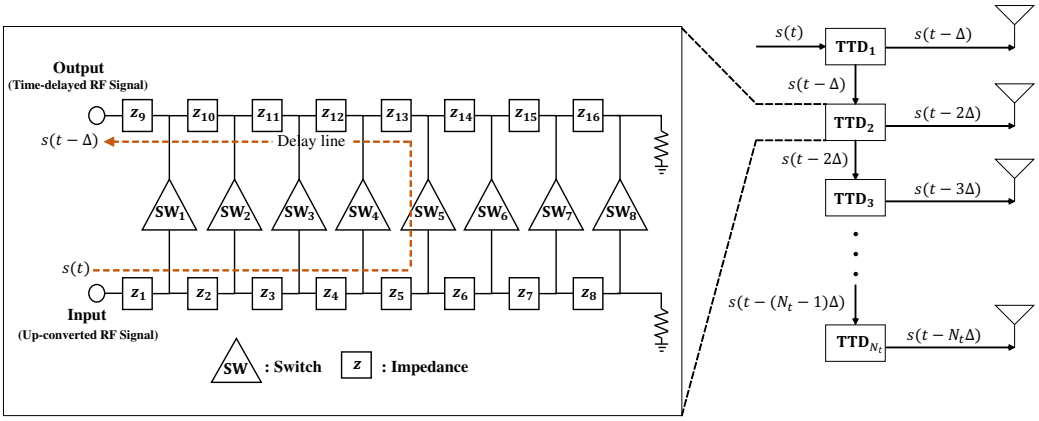

Fig. 1: Structure of a 3-bit TTD and TTD array. The time delay is $\Delta = \frac{L}{c}$ where L is the length of the dotted delay line and c is the propagation speed of RF signal.

a device consisting of multiple switches and electrical impedances, to change the phase of the RF signal. As illustrated in Fig. 1, when the fifth switch SW_5 is activated, the RF signal will propagate through the dotted delay line and the phase shift being proportional to the product of time delay $\Delta = \frac{L}{c}$ and the signal frequency f_i is induced. Specifically, if a time delay Δ is induced to an input RF signal (i.e., a sum of subcarrier signals) $s(t) = \sum_{i=1}^{S} s_i(t) = \sum_{i=1}^{S} s_i e^{j2\pi f_i t}$, then the output RF signal will be $s(t-\Delta) = \sum_{i=1}^{S} s_i e^{j2\pi f_i (t-\Delta)} = \sum_{i=1}^{S} s_i(t) e^{-j2\pi f_i \Delta}$ so that the frequency-dependent phase shift $-2\pi f_i \Delta$ is induced for each subcarrier signal $s_i(t)$.

Using the multiple TTD-based phase shifters, say N TTDs, one can generate multiple frequency-dependent beams, each of which is heading toward the distinct direction. Specifically, let $x_{i,n}(t,\tau)$ be an output of the n-th TTD for the i-th subcarrier signal, then $x_{i,n}(t,\tau)$ can be expressed as $x_{i,n}(t,\tau) = s_i(t-(n-1)\tau) = s_i(t)e^{-j(n-1)2\pi f_i \tau}$. By stacking $x_{i,n}(t,\tau)$ of all N TTDs, one can express the output vector $\mathbf{x}_i(t)$ of TTDs for the i-th subcarrier signal as

$$\mathbf{x}_i(t) = [x_{i,1}(t,\tau) \cdots x_{i,N}(t,\tau)]^{\mathrm{T}} \tag{6}$$

$$= \left[1 \cdots e^{-j(N-1)\pi f_i \tau}\right]^{\mathrm{T}} s_i(t) \tag{7}$$

$$= \mathbf{f}_i(\tau) s_i(t). \tag{8}$$

From this relationship, one can see that $\mathbf{f}_i(\tau) = \left[1\, e^{-j2\pi f_i \tau} \cdots e^{-j(N-1)2\pi f_i \tau}\right]^{\mathrm{T}} = \mathbf{a}_N(-2\pi f_i \tau)$ is the TTD beamforming vector at the i-th subcarrier. One can also see that the spatial direction of $\mathbf{f}_i(\tau)$ is $-2\pi f_i \tau$, which is the function of the subcarrier frequency f_i. In summary, using the TTD-based phase shifters, one can generate S distinct beams $\{\mathbf{f}_i(\tau)\}_{i=1}^{S}$ (S is the number of subcarriers), each of which is heading toward the distinct directions.

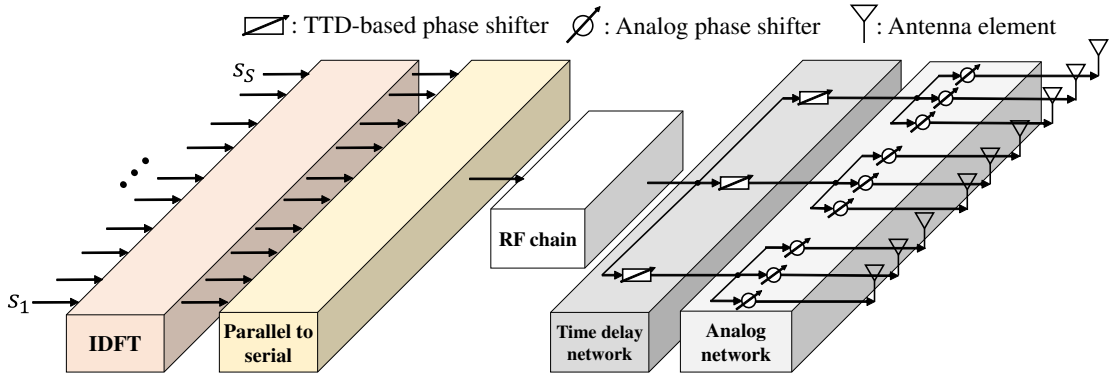

Fig. 2: Overall structure of the conventional DPP scheme.

C. Conventional Delay-phased Precoding

To simultaneously generate the multiple training beams heading toward the desired directions, DPP employs both TTDs and analog phase shifters [18], [22]. Let N and T be the numbers of analog phase shifters and TTDs, then each TTD is connected to $P = \frac{N}{T}$ analog phase shifters (see Fig. 2). The DPP beamforming vector $\mathbf{f}_i^{\text{dpp}} \in \mathbb{C}^N$ at the i-th subcarrier is

$$\mathbf{f}_i^{\text{dpp}} = \mathbf{f}^{\text{ana}}(\theta) \odot \mathbf{f}_i^{\text{td}}(\tau), \quad i = 1, \cdots, S, \tag{9}$$

where $\mathbf{f}^{\text{ana}}(\theta) \in \mathbb{C}^N$ is the beamforming vector generated by the analog phase shifters:

$$\mathbf{f}^{\text{ana}}(\theta) = [1\, e^{j\theta} \cdots e^{j(N-1)\theta}]^{\text{T}}, \tag{10}$$

and $\mathbf{f}_i^{\text{td}}(\tau) \in \mathbb{C}^N$ is the beamforming vector generated by the TTDs:

$$\mathbf{f}_i^{\text{td}}(\tau) = \left[1\, e^{-j2\pi f_i \tau} \cdots e^{-j(T-1)2\pi f_i \tau}\right]^{\text{T}} \otimes \mathbf{1}_P, \tag{11}$$

where τ is the time delay provided by the TTDs. Noting that $\mathbf{f}^{\text{ana}}(\theta) = \mathbf{a}_N(\theta)$ and $\mathbf{f}_i^{\text{td}}(\tau) = \mathbf{a}_T(-2\pi f_i \tau) \otimes \mathbf{1}_P$, one can re-express $\mathbf{f}_i^{\text{dpp}}$ as

$$\begin{aligned}
\mathbf{f}_i^{\text{dpp}} &= \mathbf{a}_N(\theta) \odot (\mathbf{a}_T(-2\pi f_i \tau) \otimes \mathbf{1}_P) && (12)\\
&\overset{(a)}{=} (\mathbf{a}_T(P\theta) \otimes \mathbf{a}_P(\theta)) \odot (\mathbf{a}_T(-2\pi f_i \tau) \otimes \mathbf{1}_P) && (13)\\
&\overset{(b)}{=} (\mathbf{a}_T(P\theta) \odot \mathbf{a}_T(-2\pi f_i \tau)) \otimes (\mathbf{a}_P(\theta) \odot \mathbf{1}_P) && (14)\\
&\overset{(c)}{=} \mathbf{a}_T(P\theta - 2\pi f_i \tau) \otimes \mathbf{a}_P(\theta), && (15)
\end{aligned}$$

where (a), (b), and (c) follow from $\mathbf{a}_N(\theta) = \mathbf{a}_T(P\theta) \otimes \mathbf{a}_P(\theta)$, $(\mathbf{A} \otimes \mathbf{B}) \odot (\mathbf{C} \otimes \mathbf{D}) = (\mathbf{A} \odot \mathbf{C}) \otimes (\mathbf{B} \odot \mathbf{D})$, and $\mathbf{a}_N(\theta) \odot \mathbf{a}_N(\phi) = \mathbf{a}_N(\theta + \phi)$, respectively[4].

[4]For example, when $N = 6$, $T = 2$, and $P = 3$, then $\mathbf{a}_N(\theta)$ can be re-expressed as $\mathbf{a}_6(\theta) = [1\, e^{j\theta} \cdots e^{j5\theta}]^{\text{T}} = [[1\, e^{j\theta}\, e^{j2\theta}]^{\text{T}}\ e^{j3\theta}[1\, e^{j\theta}\, e^{j2\theta}]^{\text{T}}] = [1\, e^{j3\theta}]^{\text{T}} \otimes [1\, e^{j\theta}\, e^{j2\theta}]^{\text{T}} = \mathbf{a}_2(3\theta) \otimes \mathbf{a}_3(\theta)$.

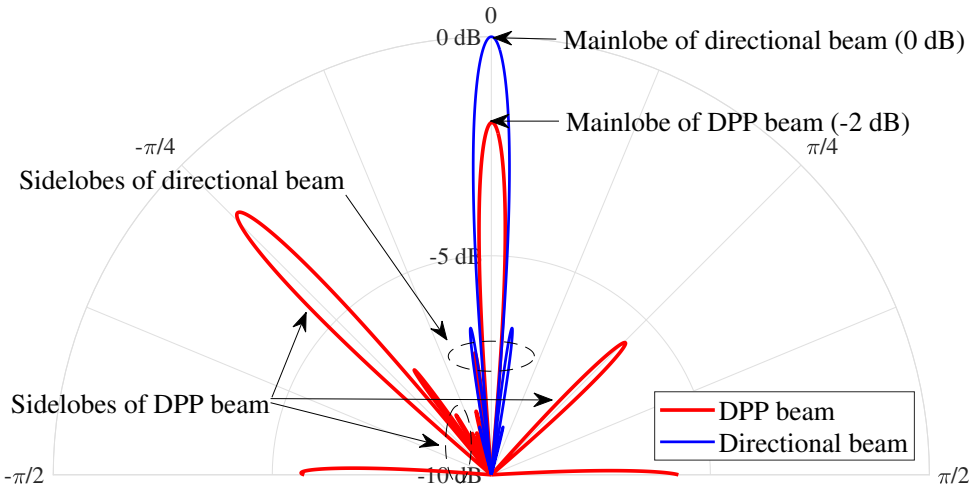

Fig. 3: Beam patterns of DPP beam and directional beam ($N = 32$, $f_c = 100\,\text{GHz}$, $B = 10\,\text{GHz}$, $S = 16$, $T = 8$, $P = 4$, $\theta = -0.25$, and $\tau = -4.2 \times 10^{-10}$). One can see that the sidelobe leakage of the DPP beam is much larger than that of the directional beam.

By properly controlling τ and θ, one can generate S DPP beams $\{\mathbf{f}_i^{\text{dpp}}\}_{i=1}^{S}$ directed to the desired directions. However, due to the Kronecker product in (15), one cannot easily guess the spatial direction of $\mathbf{f}_i^{\text{dpp}}$. By the spatial direction, we mean the direction of the array steering vector having the highest correlation with $\mathbf{f}_i^{\text{dpp}}$. Put it formally, the spatial direction θ_i of $\mathbf{f}_i^{\text{dpp}}$ is defined as $\theta_i = \arg\max_{\theta'} \left|\mathbf{a}_N^{\text{H}}(\theta')\mathbf{f}_i^{\text{dpp}}\right|^2$.

Lemma 1. *The spatial direction θ_i of the DPP beamforming vector $\mathbf{f}_i^{\text{DPP}}$ is $\theta_i = \theta - \frac{2\pi f_i \tau}{P}$ [18].*

Due to the partially-connected structure where one TTD is connected to multiple analog phase shifters, DPP cannot generate sharp training beams. To measure the difference between the DPP beamforming vector $\mathbf{f}_i^{\text{dpp}}$ and the desired directional beamforming vector $\mathbf{a}_N(\theta_i)$, one can re-express $\mathbf{a}_N(\theta_i)$ as

$$\mathbf{a}_N(\theta_i) = \mathbf{a}_T(P\theta_i) \otimes \mathbf{a}_P(\theta_i) \tag{16}$$

$$\overset{(a)}{=} \mathbf{a}_T(P\theta - 2\pi f_i \tau) \otimes \mathbf{a}_P\Big(\theta - \frac{2\pi f_i \tau}{P}\Big), \tag{17}$$

where (a) is from Lemma 1. It is clear from (15) and (17) that $\mathbf{f}_i^{\text{dpp}}$ and $\mathbf{a}_N(\theta_i)$ are not the same due to the difference between $\mathbf{a}_P\big(\theta - \frac{2\pi f_i \tau}{P}\big)$ and $\mathbf{a}_P(\theta)$, which implies that the signal power is not fully concentrated onto the mainlobe. Power leakage of the sidelobes causes a considerable degradation of beamforming gain. To quantify this behavior, we evaluate the beamforming gain

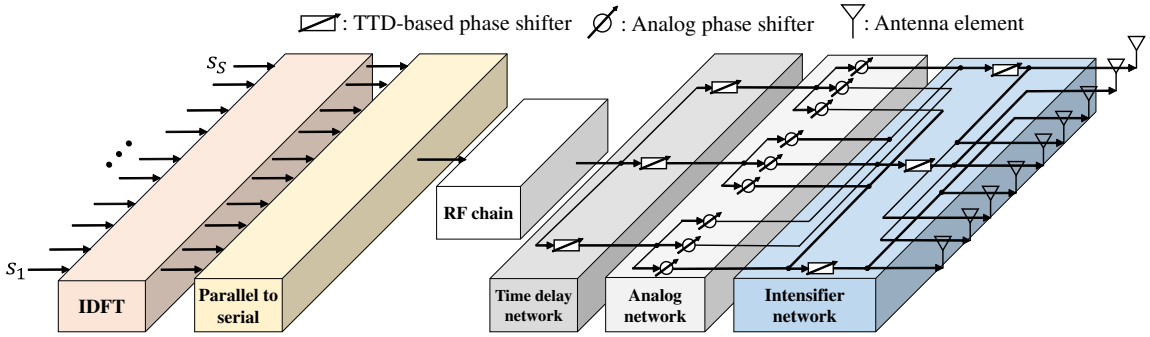

Fig. 4: Overall structure of the proposed FDB scheme.

$G_i^{\text{dpp}} = |\frac{1}{N}\mathbf{a}_N^{\text{H}}(\theta_i)\mathbf{f}_i^{\text{dpp}}|^2$ of the DPP beam $\mathbf{f}_i^{\text{dpp}}$ at the i-th subcarrier channel:

$$G_i^{\text{dpp}} = \left|\frac{1}{N}\mathbf{a}_N^{\text{H}}(\theta_i)\mathbf{f}_i^{\text{dpp}}\right|^2 \tag{18}$$

$$= \left|\frac{1}{N}\Big(\mathbf{a}_T(P\theta - 2\pi f_i\tau) \otimes \mathbf{a}_P\Big(\theta - \frac{2\pi f_i\tau}{P}\Big)\Big)^{\text{H}}\big(\mathbf{a}_T(P\theta - 2\pi f_i\tau) \otimes \mathbf{a}_P(\theta)\big)\right|^2 \tag{19}$$

$$= \left|\frac{1}{P}\mathbf{a}_P^{\text{H}}\Big(\theta - \frac{2\pi f_i\tau}{P}\Big)\mathbf{a}_P(\theta)\right|^2 \tag{20}$$

$$= \left|\frac{\sin(\pi f_i\tau)}{P\sin\frac{\pi f_i\tau}{P}}\right|^2. \tag{21}$$

One can see that G_i^{dpp} is a function of τ and achieves the maximum value at $\tau = 0$. If $\tau = 0$, then the spatial directions of all DPP beams will be the same ($\theta_i = \theta - \frac{2\pi f_i\tau}{P} = \theta$) so that the BS would simply search one direction at a time. If $\tau \neq 0$, there would be a degradation in the beamforming gain G_i^{dpp}. Indeed, as shown in Fig. 3, the mainlobe of the DPP beam $\mathbf{f}_i^{\text{dpp}}$ is 2 dB lower than that of the desired directional beam $\mathbf{a}_N(\theta_i)$.

III. Frequency-dependent Beamforming for Wideband Terahertz Systems

Main purpose of the proposed FDB is to simultaneously generate multiple frequency-dependent beams achieving the maximum beamforming gain. To this end, FDB employs three signal propagation networks (see Fig. 4): 1) *time delay network* generating frequency-dependent beams using the TTD-based phase shifters, 2) *analog network* changing the spatial directions of the beams generated by the time delay network, 3) *intensifier network* suppressing the sidelobes of the subcarrier beams generated by the time delay network and the analog network. Key ingredient of FDB is the intensifier network compensating for the difference between the FDB beam and the desired directional beam. By generating very sharp training beams, the received power of the beam aligned with the channel propagation path gets larger while those of the misaligned beams get smaller, resulting in a significant improvement of the beamforming gain.

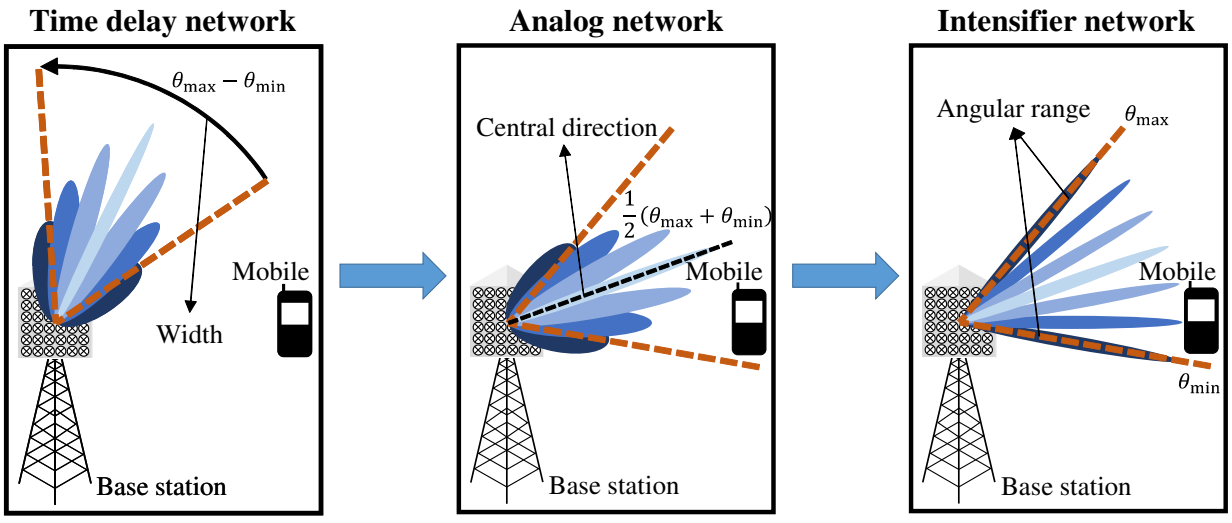

Fig. 5: FDB beam generation via time delay network, analog network, and intensifier network.

A. *Overall Operation of Frequency-dependent Beamforming*

The FDB beamforming vector $\mathbf{f}_i \in \mathbb{C}^N$ constructed by the time delay network, analog network, and intensifier network can be expressed as

$$\mathbf{f}_i = \mathbf{f}_i^{\text{it}}(\eta) \odot \mathbf{f}^{\text{ana}}(\theta) \odot \mathbf{f}_i^{\text{td}}(\tau), \quad i = 1, \cdots, S, \tag{22}$$

where θ is the phase shift of the analog phase shifters and τ and η are the time delays provided by the TTDs in the time delay network and intensifier network, respectively. Also, $\mathbf{f}_i^{\text{td}}(\tau), \mathbf{f}^{\text{ana}}(\theta), \mathbf{f}_i^{\text{it}}(\eta) \in \mathbb{C}^N$ are the beamforming vectors generated by the time delay network, analog network, and intensifier network, respectively. By deliberately controlling the FDB parameters (τ, θ, η), the BS can generate $\{\mathbf{f}_i\}_{i=1}^S$ directed to the desired probing area $[\theta_{\min}, \theta_{\max}]$.

We start by defining the notions used in our beamforming algorithm design. First, the angular range of $\{\mathbf{f}_i\}_{i=1}^S$ is defined as

$$\text{Range}(\{\mathbf{f}_i\}_{i=1}^S) = \left[\theta_1, \theta_S\right], \tag{23}$$

where $\theta_i = \arg\max_\theta |\mathbf{a}_N^{\text{H}}(\theta)\mathbf{f}_i|^2$ is the spatial direction of $\mathbf{f}_i$. Note that $\text{Range}(\{\mathbf{f}_i\}_{i=1}^S)$ is a function of the central direction and the width, defined by

$$\text{Center}(\{\mathbf{f}_i\}_{i=1}^S) = \frac{1}{2}(\theta_1 + \theta_S), \tag{24}$$

$$\text{Width}(\{\mathbf{f}_i\}_{i=1}^S) = \theta_S - \theta_1. \tag{25}$$

Thus, to enforce Range$(\{\mathbf{f}_i\}_{i=1}^S) = [\theta_{\min}, \theta_{\max}]$, we should set Center$(\{\mathbf{f}_i\}_{i=1}^S) = \frac{1}{2}(\theta_{\min} + \theta_{\max})$ and Width$(\{\mathbf{f}_i\}_{i=1}^S) = \theta_{\max} - \theta_{\min}$.

The overall operation of FDB is as follows (see Fig. 5):

- **Time delay network**: By controlling the time delay τ in the time delay network, multiple frequency-dependent beams $\{\mathbf{f}_i^{\text{td}}(\tau)\}_{i=1}^S$ such that Width$(\{\mathbf{f}_i^{\text{td}}(\tau)\}_{i=1}^S) = \theta_{\max} - \theta_{\min}$ are generated.
- **Analog network**: By controlling the phase shift θ in the analog network, the central direction of the generated beams $\{\mathbf{f}^{\text{ana}}(\theta) \odot \mathbf{f}_i^{\text{td}}(\tau)\}_{i=1}^S$ is set to Center$(\{\mathbf{f}^{\text{ana}}(\theta) \odot \mathbf{f}_i^{\text{td}}(\tau)\}_{i=1}^S) = \frac{1}{2}(\theta_{\min} + \theta_{\max})$ while maintaining the width.
- **Intensifier network**: By controlling the time delay η in the intensifier network, we can bridge the gap between the FDB beamforming vectors $\{\mathbf{f}_i^{\text{it}}(\eta) \odot \mathbf{f}^{\text{ana}}(\theta) \odot \mathbf{f}_i^{\text{td}}(\tau)\}_{i=1}^S$ and the desired directional beamforming vectors $\{\mathbf{a}_N(\theta_i)\}_{i=1}^S$.

B. Frequency-dependent Beam Generation

In this subsection, we explain the detailed operation of the FDB beam generation.

1) Time Delay Network: To generate the multiple frequency-dependent beams, we employ $T(< N)$ TTDs, each of which is connected to $P = \frac{N}{T}$ phase shifters in the analog network. The time delay network beamforming vector $\mathbf{f}_i^{\text{td}}(\tau)$ at the i-th subcarrier is

$$\mathbf{f}_i^{\text{td}}(\tau) = [1\, e^{-j2\pi f_i \tau} \cdots e^{-j(T-1)2\pi f_i \tau}]^{\text{T}} \otimes \mathbf{1}_P = \mathbf{a}_T(-2\pi f_i \tau) \otimes \mathbf{1}_P. \tag{26}$$

Using Lemma 1, one can see that the spatial direction of $\mathbf{f}_i^{\text{td}}(\tau)$ is $-\frac{2\pi f_i \tau}{P}$. For example, the spatial direction of the first subcarrier beam $\mathbf{f}_1^{\text{td}}(\tau)$ is $-\frac{2\pi f_1 \tau}{P}$ and that of the last subcarrier beam $\mathbf{f}_S^{\text{td}}(\tau)$ is $-\frac{2\pi f_S \tau}{P}$. Since Width$(\{\mathbf{f}_i^{\text{td}}\}_{i=1}^S) = -\frac{2\pi\tau}{P}(f_S - f_1)$, by setting τ as

$$\tau = -\frac{P(\theta_{\max} - \theta_{\min})}{2\pi(f_S - f_1)} = -\frac{P(\theta_{\max} - \theta_{\min})}{2\pi B}, \tag{27}$$

we can enforce Width$(\{\mathbf{f}_i^{\text{td}}(\tau)\}_{i=1}^S) = \theta_{\max} - \theta_{\min}$. Note that the central direction of the generated beams $\{\mathbf{f}_i^{\text{td}}(\tau)\}_{i=1}^S$ is Center$(\{\mathbf{f}_i^{\text{td}}(\tau)\}_{i=1}^S) = -\frac{\pi(f_1+f_S)\tau}{P} = \frac{f_1+f_S}{2B}(\theta_{\max} - \theta_{\min})$.

2) Analog Network: In the analog network, the central direction $\frac{f_1+f_S}{2B}(\theta_{\max} - \theta_{\min})$ of the beams generated from the time delay network is changed to $\frac{1}{2}(\theta_{\min} + \theta_{\max})$. The analog beamforming vector $\mathbf{f}^{\text{ana}}(\theta)$ is

$$\mathbf{f}^{\text{ana}}(\theta) = [1\, e^{j\theta} \cdots e^{j(N-1)\theta}]^{\text{T}} = \mathbf{a}_N(\theta). \tag{28}$$

Using (26)-(28), the i-th subcarrier beam $\mathbf{f}^{\text{ana}}(\theta) \odot \mathbf{f}_i^{\text{td}}(\tau)$ generated by the time delay network and analog network can be expressed as

$$\mathbf{f}^{\text{ana}}(\theta) \odot \mathbf{f}_i^{\text{td}}(\tau) = \mathbf{a}_N(\theta) \odot (\mathbf{a}_T(-2\pi f_i \tau) \otimes \mathbf{1}_P) \tag{29}$$

$$= (\mathbf{a}_T(P\theta) \otimes \mathbf{a}_P(\theta)) \odot (\mathbf{a}_T(-2\pi f_i \tau) \otimes \mathbf{1}_P) \tag{30}$$

$$= \mathbf{a}_T(P\theta - 2\pi f_i \tau) \otimes \mathbf{a}_P(\theta) \tag{31}$$

$$\overset{(a)}{=} \mathbf{a}_T\Big(P\theta + \frac{Pf_i}{B}(\theta_{\text{max}} - \theta_{\text{min}})\Big) \otimes \mathbf{a}_P(\theta), \tag{32}$$

where (a) is from (27). One can see from Lemma 1 and (32) that the spatial direction of $\mathbf{f}^{\text{ana}}(\theta) \odot \mathbf{f}_i^{\text{td}}(\tau)$ is $\theta + \frac{f_i}{B}(\theta_{\text{max}} - \theta_{\text{min}})$. Since Center$(\{\mathbf{f}^{\text{ana}}(\theta) \odot \mathbf{f}_i^{\text{td}}(\tau)\}_{i=1}^S) = \theta + \frac{f_1+f_S}{2B}(\theta_{\text{max}} - \theta_{\text{min}})$, by setting θ as

$$\theta = \frac{1}{2}(\theta_{\text{min}} + \theta_{\text{max}}) - \frac{f_1 + f_S}{2B}(\theta_{\text{max}} - \theta_{\text{min}}) = \frac{f_S\theta_{\text{min}} - f_1\theta_{\text{max}}}{B}, \tag{33}$$

we can enforce Center$(\{\mathbf{f}^{\text{ana}}(\theta) \odot \mathbf{f}_i^{\text{td}}(\tau)\}_{i=1}^S) = \frac{1}{2}(\theta_{\text{min}} + \theta_{\text{max}})$.

In summary, by setting τ and θ as (27) and (33), respectively, we can set the angular range of $\{\mathbf{f}^{\text{ana}}(\theta) \odot \mathbf{f}_i^{\text{td}}(\tau)\}_{i=1}^S$ to $[\theta_{\text{min}}, \theta_{\text{max}}]$.

3) Intensifier Network: Although the angular range of the generated beams is set to the desired probing area $[\theta_{\text{min}}, \theta_{\text{max}}]$, the generated beams suffer from a severe degradation of beamforming gain due to the high sidelobe leakage (see (18)-(21)). Main purpose of the intensifier network is to concentrate the signal power to the mainlobe by closing the gap between the FDB beam $\mathbf{f}_i$ and the desired directional beamforming vector $\mathbf{a}_N(\theta_i)$ (θ_i is the spatial direction of $\mathbf{f}_i$).

Basically, the intensifier network consists of P TTDs, each of which is connected to $T = \frac{N}{P}$ analog phase shifters. The intensifier beamforming vector $\mathbf{f}_i^{\text{it}}(\eta)$ at the i-th subcarrier is

$$\mathbf{f}_i^{\text{it}}(\eta) = \mathbf{1}_T \otimes [1\, e^{-j2\pi f_i \eta} \cdots e^{-j(P-1)2\pi f_i \eta}]^{\text{T}} = \mathbf{1}_T \otimes \mathbf{a}_P(-2\pi f_i \eta). \tag{34}$$

Substituting (32) and (34) into (22), the FDB beam $\mathbf{f}_i$ can be re-expressed as

$$\mathbf{f}_i = \mathbf{f}_i^{\text{it}}(\eta) \odot \mathbf{f}^{\text{ana}}(\theta) \odot \mathbf{f}_i^{\text{td}}(\tau) \tag{35}$$

$$= (\mathbf{1}_T \otimes \mathbf{a}_P(-2\pi f_i \eta)) \odot \Big(\mathbf{a}_T\Big(P\theta + \frac{Pf_i}{B}(\theta_{\text{max}} - \theta_{\text{min}})\Big) \otimes \mathbf{a}_P(\theta)\Big) \tag{36}$$

$$= \mathbf{a}_T\Big(P\theta + \frac{Pf_i}{B}(\theta_{\text{max}} - \theta_{\text{min}})\Big) \otimes \mathbf{a}_P(\theta - 2\pi f_i \eta) \tag{37}$$

$$\overset{(a)}{=} \mathbf{a}_T\Big(P\Big(\theta_{\text{min}} + \frac{i-1}{S-1}(\theta_{\text{max}} - \theta_{\text{min}})\Big)\Big) \otimes \mathbf{a}_P\Big(\frac{f_S\theta_{\text{min}} - f_1\theta_{\text{max}}}{B} - 2\pi f_i \eta\Big). \tag{38}$$

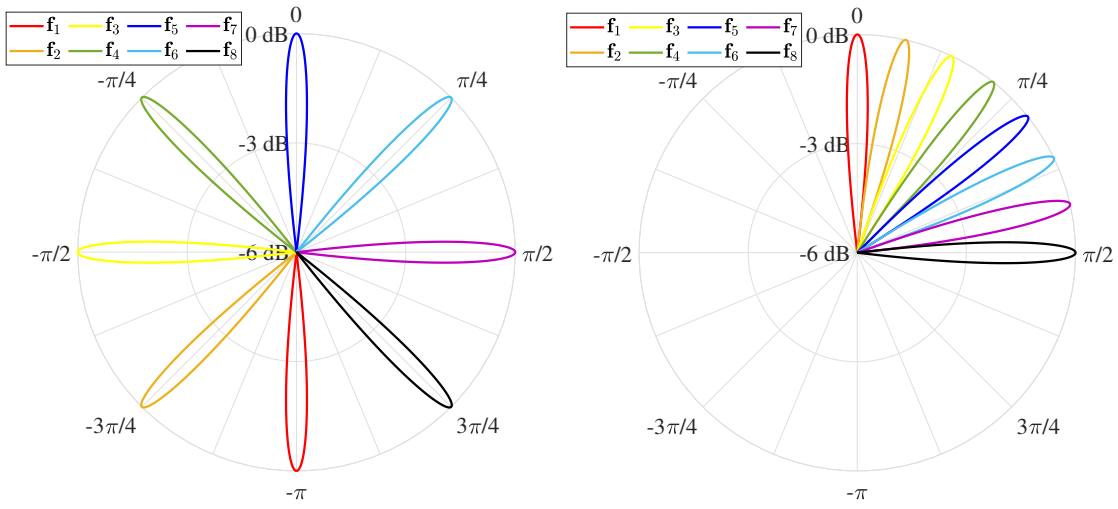

Fig. 6: Beam patterns of FDB beams when (a) $[\theta_{\min}, \theta_{\max}] = [-\pi, \frac{3\pi}{4}]$ and (b) $[\theta_{\min}, \theta_{\max}] = [0, \frac{\pi}{2}]$.

where (a) is from (27) and (33). From Lemma 1, one can see that the spatial direction θ_i of $\mathbf{f}_i$ is given by

$$\theta_i = \theta_{\min} + \frac{i-1}{S-1}(\theta_{\max} - \theta_{\min}). \tag{39}$$

Using this, $\mathbf{f}_i$ in (38) can be re-expressed as

$$\mathbf{f}_i = \mathbf{a}_T(P\theta_i) \otimes \mathbf{a}_P\Big(\theta_i - \frac{f_i}{B}(\theta_{\max} - \theta_{\min}) - 2\pi f_i \eta\Big). \tag{40}$$

Also, the desired directional beamforming vector $\mathbf{a}_N(\theta_i)$ can be expressed as

$$\mathbf{a}_N(\theta_i) = \mathbf{a}_T(P\theta_i) \otimes \mathbf{a}_P(\theta_i). \tag{41}$$

From (40) and (41), one can easily see that η satisfying $\mathbf{f}_i = \mathbf{a}_N(\theta_i)$ is

$$\eta = -\frac{\theta_{\max} - \theta_{\min}}{2\pi B}. \tag{42}$$

In summary, by setting the FDB parameters (τ, θ, η) as (27), (33), and (42), one can generate S FDB beams $\{\mathbf{f}_i\}_{i=1}^S$ directed toward the desired probing area $[\theta_{\min}, \theta_{\max}]$. As shown in Fig. 6, these beams achieve the maximum beamforming gain $G_i^{\text{fdb}} = \left|\frac{1}{N}\mathbf{a}_N^{\text{H}}(\theta_i)\mathbf{f}_i\right|^2 = \left|\frac{1}{N}\mathbf{a}_N^{\text{H}}(\theta_i)\mathbf{a}_N(\theta_i)\right|^2 = 1$.

IV. Frequency-dependent Beamforming-based Terahertz Beam Management

As mentioned, the conventional beam management scheme is based on the analog phase shifters, so that the BS can search only one direction at a time. To speed up the beam management process, we propose the FDB-based beam management strategy that simultaneously searches

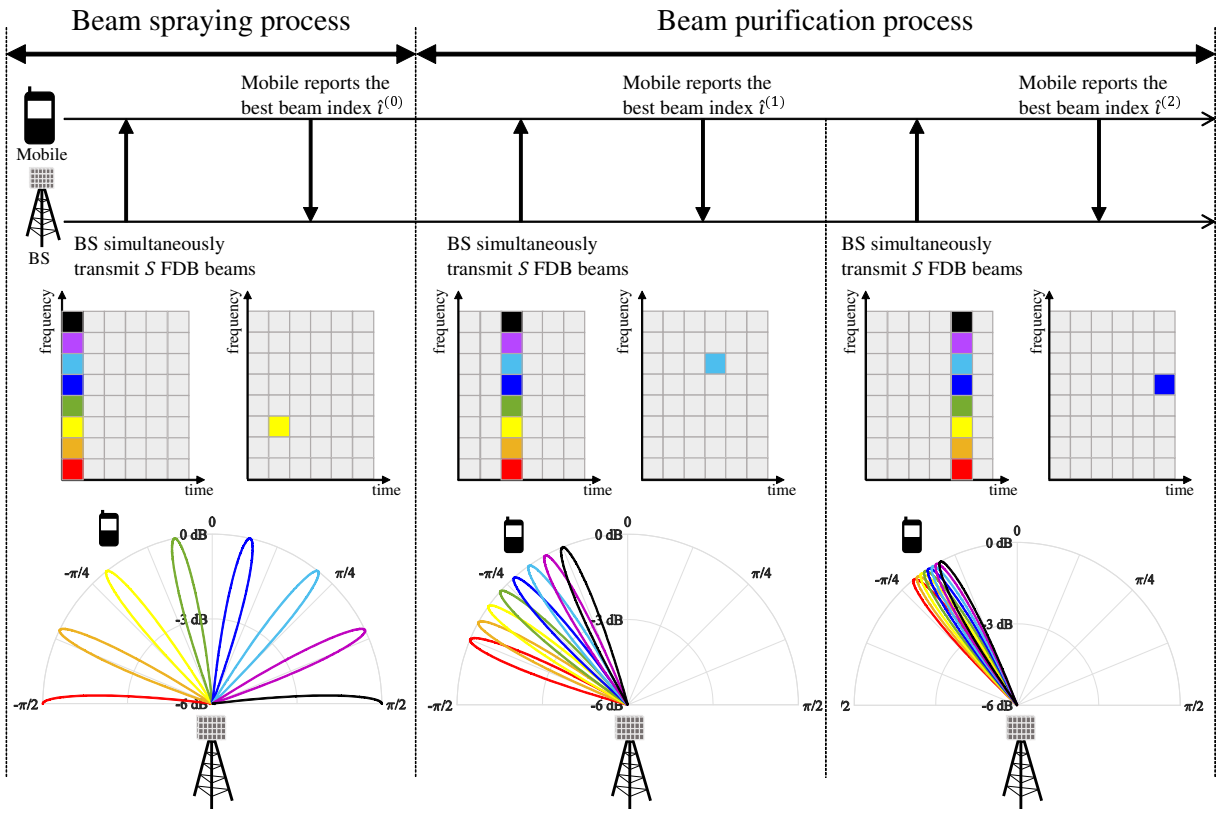

Fig. 7: Illustration of the proposed FDB-based beam management.

multiple directions using the frequency-dependent beams. The essence of the proposed scheme is to deliberately design the FDB parameters, i.e., the time delay of the time delay network τ (see (27)), the phase shift of the analog network θ (see (33)), the time delay of the intensifier network η (see (42)), to generate the FDB beams directed to the desired probing area. Since the number of FDB beams is the same as the number of subcarriers in the wideband THz systems (e.g., $64 \sim 256$), we can achieve a significant reduction in the beam management latency. Also, since the sidelobe levels of the FDB beams are properly suppressed by the intensifier network, the probability to find out the optimal beam direction increases significantly.

The proposed scheme consists of two major operational steps (see Fig. 7). In the first step called *beam spraying*, the BS simultaneously transmits the FDB beams directed to the whole angular area and the mobile feeds back the index of the FDB beam maximizing the RSRP to the BS. In the second step called *beam purification*, to find out the precise beam direction, the BS performs the fine-tuning to the narrow angular area identified in the first step[5].

[5]Note that to narrow down the beam direction, one can perform multiple beam purification processes.

A. Beam Spraying Process

In the beam spraying process, to acquire the rough estimates of the subcarrier channel directions $\{\phi_i\}_{i=1}^S$, the BS transmits the FDB beams $\mathbf{f}_1^{(0)}, \cdots, \mathbf{f}_S^{(0)}$ whose spatial directions are uniformly distributed in $\big[-\pi, -\pi+\frac{2\pi(S-1)}{S}\big]$. This task is performed by setting the FDB parameters as

$$(\tau^{(0)}, \theta^{(0)}, \eta^{(0)}) = \Big(-\frac{P(S-1)}{BS}, -\pi - \frac{2\pi f_1(S-1)}{BS}, -\frac{S-1}{BS}\Big). \tag{43}$$

In doing so, the generated FDB beam $\mathbf{f}_i^{(0)}$ at the i-th subcarrier is directed toward the spatial direction $\theta_i^{(0)} = -\pi + \frac{2\pi}{S}(i-1) \in [-\pi, \pi]$ (see (39)). After the FDB beam generation, the BS simultaneously transmits $\{\mathbf{f}_i^{(0)}\}_{i=1}^S$ carrying the reference signal. Then the received signal $y_i^{(0)}$ of the mobile at the i-th subcarrier is given by

$$y_i^{(0)} = \mathbf{h}_i^{\mathrm{H}} \mathbf{f}_i^{(0)} s + n_i^{(0)}, \quad i = 1, \cdots, S, \tag{44}$$

where s is the pilot symbol and n_i is additive Gaussian noise. The mobile feeds back the subcarrier index $\hat{i}^{(0)}$ of the FDB beam $\mathbf{f}_{\hat{i}^{(0)}}^{(0)}$ maximizing the RSRP to the BS as

$$\hat{i}^{(0)} = \arg \max_{i=1,\cdots,S} \big|y_i^{(0)}\big|^2. \tag{45}$$

Since the RSRP is maximized only when the FDB beamforming vectors are properly aligned with the subcarrier channel vectors, the BS can acquire the estimates of the subcarrier channel directions $\{\phi_i\}_{i=1}^S$ from the FDB beam index feedback $\hat{i}^{(0)}$.

Lemma 2. *The angular area of the carrier channel direction $\phi_c = \pi \sin\varphi$ designated by the chosen FDB beam $\mathbf{f}_{\hat{i}^{(0)}}$ is given by $\left[\frac{\left(\theta_{\hat{i}^{(0)}}^{(0)}+\theta_{\hat{i}^{(0)}-1}^{(0)}\right)f_c}{f_{\hat{i}^{(0)}}+f_{\hat{i}^{(0)}-1}}, \frac{\left(\theta_{\hat{i}^{(0)}}^{(0)}+\theta_{\hat{i}^{(0)}+1}^{(0)}\right)f_c}{f_{\hat{i}^{(0)}}+f_{\hat{i}^{(0)}+1}}\right]$. Also, using $\phi_i = \frac{f_i}{f_c}\phi_c$, the subcarrier channel directions $\{\phi_i\}_{i=1}^S$ can be bounded as*

$$\frac{\left(\theta_{\hat{i}^{(0)}}^{(0)} + \theta_{\hat{i}^{(0)}-1}^{(0)}\right) f_i}{f_{\hat{i}^{(0)}} + f_{\hat{i}^{(0)}-1}} \le \phi_i \le \frac{\left(\theta_{\hat{i}^{(0)}}^{(0)} + \theta_{\hat{i}^{(0)}+1}^{(0)}\right) f_i}{f_{\hat{i}^{(0)}} + f_{\hat{i}^{(0)}+1}}, \quad i = 1, \cdots, S. \tag{46}$$

Proof. See Appendix A. □

Due to the large number of subcarriers S in the wideband THz systems (e.g., $S = 128 \sim 512$), the angular area covered by the FDB beam is much smaller than that of the conventional synchronization signal block (SSB) beam used in the beam sweeping process of 5G NR. In fact, in 5G NR, up to 64 SSB beams are transmitted so that the angular area covered by each SSB beam is around $\frac{360^\circ}{64} \approx 5.6^\circ$ [19]. In contrast, when $S = 256$, the angular area covered by each FDB beam is around $\frac{360^\circ}{256} \approx 1.4^\circ$, which is 4 times sharper than that of each SSB beam.

From Lemma 2, one can easily see that the range of $\{\phi_i\}_{i=1}^S$ is $\left[\frac{\left(\theta_{\hat{i}(0)}^{(0)}+\theta_{\hat{i}(0)-1}^{(0)}\right)f_1}{f_{\hat{i}(0)}+f_{\hat{i}(0)-1}}, \frac{\left(\theta_{\hat{i}(0)}^{(0)}+\theta_{\hat{i}(0)+1}^{(0)}\right)f_S}{f_{\hat{i}(0)}+f_{\hat{i}(0)+1}}\right]$ if $\frac{\theta_{\hat{i}(0)}^{(0)}+\theta_{\hat{i}(0)+1}^{(0)}}{f_{\hat{i}(0)}+f_{\hat{i}(0)+1}} \geq 0$ and $\left[\frac{\left(\theta_{\hat{i}(0)}^{(0)}+\theta_{\hat{i}(0)+1}^{(0)}\right)f_S}{f_{\hat{i}(0)}+f_{\hat{i}(0)+1}}, \frac{\left(\theta_{\hat{i}(0)}^{(0)}+\theta_{\hat{i}(0)-1}^{(0)}\right)f_1}{f_{\hat{i}(0)}+f_{\hat{i}(0)-1}}\right]$ otherwise. After the beam spraying process, the BS transmits the FDB beams toward $\left[\frac{\left(\theta_{\hat{i}(0)}^{(0)}+\theta_{\hat{i}(0)-1}^{(0)}\right)f_1}{f_{\hat{i}(0)}+f_{\hat{i}(0)-1}}, \frac{\left(\theta_{\hat{i}(0)}^{(0)}+\theta_{\hat{i}(0)+1}^{(0)}\right)f_S}{f_{\hat{i}(0)}+f_{\hat{i}(0)+1}}\right]$ to narrow down the beam direction.

B. Beam Purification Process

In the beam purification process, to find out the precise beam direction, the BS transmits the FDB beams toward the angular area determined by the beam spraying process. In essence, the beam purification process is similar to the beam spraying process in the sense that the FDB beams are transmitted to the probing area. The difference is that the probing area of the beam spraying process is the whole angular area while that of the beam purification process is the narrow angular area designated by the FDB beam chosen at the beam spraying process.

Specifically, the FDB beams $\mathbf{f}_1^{(1)}, \cdots, \mathbf{f}_S^{(1)}$ directed to $\left[\frac{\left(\theta_{\hat{i}(0)}^{(0)}+\theta_{\hat{i}(0)-1}^{(0)}\right)f_1}{f_{\hat{i}(0)}+f_{\hat{i}(0)-1}}, \frac{\left(\theta_{\hat{i}(0)}^{(0)}+\theta_{\hat{i}(0)+1}^{(0)}\right)f_S}{f_{\hat{i}(0)}+f_{\hat{i}(0)+1}}\right]$ are generated by setting the FDB parameters as

$$(\tau^{(1)}, \theta^{(1)}, \eta^{(1)}) = \left(-\frac{P(\theta_{\text{max}}^{(1)} - \theta_{\text{min}}^{(1)})}{2\pi B}, \frac{f_S\theta_{\text{min}}^{(1)} - f_1\theta_{\text{max}}^{(1)}}{B}, -\frac{\theta_{\text{max}}^{(1)} - \theta_{\text{min}}^{(1)}}{2\pi B}\right), \tag{47}$$

where $\theta_{\text{min}}^{(1)} = \frac{\left(\theta_{\hat{i}(0)}^{(0)}+\theta_{\hat{i}(0)-1}^{(0)}\right)f_1}{f_{\hat{i}(0)}+f_{\hat{i}(0)-1}}$ and $\theta_{\text{max}}^{(1)} = \frac{\left(\theta_{\hat{i}(0)}^{(0)}+\theta_{\hat{i}(0)+1}^{(0)}\right)f_S}{f_{\hat{i}(0)}+f_{\hat{i}(0)+1}}$. Note that each FDB beam $\mathbf{f}_i^{(1)}$ heads toward the spatial direction $\theta_i^{(1)} = \theta_{\text{min}}^{(1)} + \frac{i-1}{S-1}(\theta_{\text{max}}^{(1)} - \theta_{\text{min}}^{(1)}) \in [\theta_{\text{min}}^{(1)}, \theta_{\text{max}}^{(1)}]$ (see (39)). Then the received signal $y_i^{(1)}$ of the mobile at the i-th subcarrier is given by

$$y_i^{(1)} = \mathbf{h}_i^{\text{H}}\mathbf{f}_i^{(1)}s + n_i^{(1)}, \quad i = 1, \cdots, S. \tag{48}$$

After that, the mobile measures the RSRP and feeds back the subcarrier index $\hat{i}^{(1)}$ of the FDB beam $\mathbf{f}_{\hat{i}^{(1)}}^{(1)}$ maximizing the RSRP:

$$\hat{i}^{(1)} = \arg\max_{i=1,\cdots,S} \left|y_i^{(1)}\right|^2. \tag{49}$$

Using the beam index $\hat{i}^{(1)}$ fed back from the mobile, the BS can acquire the channel direction of the $\hat{i}^{(1)}$-th subcarrier as $\phi_{\hat{i}^{(1)}} = \theta_{\hat{i}^{(1)}} = \theta_{\text{min}}^{(1)} + \frac{\hat{i}^{(1)}-1}{S-1}\left(\theta_{\text{max}}^{(1)} - \theta_{\text{min}}^{(1)}\right)$. Then by exploiting the relationship $\phi_i = \frac{f_i}{f_{\hat{i}^{(1)}}}\phi_{\hat{i}^{(1)}}$, the BS can acquire the channel directions of all subcarriers as

$$\hat{\phi}_i = \frac{f_i}{f_{\hat{i}^{(1)}}}\left(\theta_{\text{min}}^{(1)} + \frac{\hat{i}^{(1)} - 1}{S-1}\left(\theta_{\text{max}}^{(1)} - \theta_{\text{min}}^{(1)}\right)\right), \quad i = 1, \cdots, S. \tag{50}$$

Note that to narrow down the beam direction, one can perform multiple beam purification processes.

Once the subcarrier channel directions are identified, the BS performs the downlink transmission (i.e., frequency-dependent data beamforming) to the mobile. The overall procedures of the FDB-based beam management are summarized in Table I.

C. Beam Misalignment Probability Analysis

In this subsection, we provide the beam misalignment probability analysis of FDB. By the beam misalignment probability, we mean the probability that the optimal beam is different from the beam chosen in the beam spraying process. For simplicity, we analyze the beam misalignment probability of the beam spraying process but the extension to the beam purification process is straightforward since the mechanical process is the same.

Let θ_i be the spatial direction of the i-th FDB beamforming vector $\mathbf{f}_i$. Then the optimal beam direction index i^* is defined as the subcarrier index of the FDB beam whose spatial direction is closest to the subcarrier channel direction:

$$i^* = \arg \min_{i=1,\cdots,S} |\theta_i - \phi_i| \tag{51}$$

$$= \arg \min_{i=1,\cdots,S} \left|\theta_i - \frac{f_i}{f_c}\frac{2\pi d \sin\varphi}{\lambda_c}\right|, \tag{52}$$

where φ is the AoD at the BS. Also, the chosen beam direction index $\hat{i}$ is defined as the subcarrier index of the FDB beam maximizing the RSRP:

$$\hat{i} = \arg \max_{i=1,\cdots,S} |y_i|^2 \tag{53}$$

$$= \arg \max_{i=1,\cdots,S} |\mathbf{h}_i^{\mathrm{H}}\mathbf{f}_i + n_i|^2 \tag{54}$$

$$= \arg \max_{i=1,\cdots,S} \left|\sqrt{\rho}\alpha_i \mathbf{a}_N^{\mathrm{H}}\Big(\frac{f_i}{f_c}\frac{2\pi d \sin\varphi}{\lambda_c}\Big)\mathbf{f}_i + n_i\right|^2. \tag{55}$$

Then the beam misalignment probability P_{miss} is defined as

$$P_{\text{miss}} = \Pr(\hat{i} \neq i^*) \tag{56}$$

$$= \Pr\big(|y_{i^*}|^2 < |y_{\hat{i}}|^2\big) \tag{57}$$

$$\overset{(a)}{=} \frac{1}{2\pi}\int_{-\pi}^{\pi} \Pr\big(|y_{i^*}|^2 < |y_{\hat{i}}|^2 \mid \varphi\big) d\varphi \tag{58}$$

$$= \frac{1}{2\pi}\int_{-\pi}^{\pi} \Pr\left(\bigcup_{\hat{i}\neq i^*}^{S} \big\{|y_{i^*}|^2 < |y_{\hat{i}}|^2\big\} \,\middle|\, \varphi\right) d\varphi, \tag{59}$$

TABLE I Frequency-dependent beamforming based THz beam management

Input: The numbers of BS and mobile antennas N and N_r, the numbers of TTDs in the time delay network and intensifier network T and P ($TP = N$), the central frequency f_c, the subcarrier frequencies $\{f_i\}_{i=1}^{S}$, the bandwidth B, the number of time slots for BS beam purification L

Beam spraying process:

$[\theta_{\min}^{(0)}, \theta_{\max}^{(0)}] = \big[-\pi, -\pi + \frac{2\pi(S-1)}{S}\big]$

$(\tau^{(0)}, \theta^{(0)}, \eta^{(0)}) = \big(-\frac{P(S-1)}{BS}, -\pi - \frac{2\pi f_1(S-1)}{BS}, -\frac{S-1}{BS}\big)$

$\theta_i^{(0)} = -\pi + \frac{2\pi}{S}(i-1), \quad i = 1, \cdots, S$

BS simultaneously transmits the FDB beams $\{\mathbf{f}_i^{(0)}\}_{i=1}^{S}$ toward $\{\theta_i^{(0)}\}_{i=1}^{S}$

$\hat{i}^{(0)} = \arg\max_{i=1,\cdots,S} \left|y_i^{(0)}\right|^2$

Mobile feeds back the subcarrier index $\hat{i}^{(0)}$ to the BS

Beam purification process:

for $l = 1, \cdots, L$ **do**

  if $\frac{\theta_{\hat{i}(0)}^{(0)} + \theta_{i(0)+1}^{(0)}}{f_{\hat{i}(0)} + f_{\hat{i}(0)+1}} \geq 0$ **then**

    $[\theta_{\min}^{(l)}, \theta_{\max}^{(l)}] = \left[\frac{\left(\theta_{\hat{i}(l-1)}^{(l-1)} + \theta_{\hat{i}(l-1)-1}^{(l-1)}\right) f_1}{f_{\hat{i}(l-1)} + f_{\hat{i}(l-1)-1}}, \frac{\left(\theta_{\hat{i}(l-1)}^{(l-1)} + \theta_{\hat{i}(l-1)+1}^{(l-1)}\right) f_S}{f_{\hat{i}(l-1)} + f_{\hat{i}(l-1)+1}}\right]$

  else

    $[\theta_{\min}^{(l)}, \theta_{\max}^{(l)}] = \left[\frac{\left(\theta_{\hat{i}(l-1)}^{(l-1)} + \theta_{\hat{i}(l-1)+1}^{(l-1)}\right) f_S}{f_{\hat{i}(l-1)} + f_{\hat{i}(l-1)+1}}, \frac{\left(\theta_{\hat{i}(l-1)}^{(l-1)} + \theta_{\hat{i}(l-1)-1}^{(l-1)}\right) f_1}{f_{\hat{i}(l-1)} + f_{\hat{i}(l-1)-1}}\right]$

  end if

  $(\tau^{(l)}, \theta^{(l)}, \eta^{(l)}) = \left(-\frac{P(\theta_{\max}^{(l)} - \theta_{\min}^{(l)})}{2\pi B}, \frac{f_S\theta_{\min}^{(l)} - f_1\theta_{\max}^{(l)}}{B}, -\frac{\theta_{\max}^{(l)} - \theta_{\min}^{(l)}}{2\pi B}\right)$

  $\theta_i^{(l)} = \theta_{\min}^{(l)} + \frac{i-1}{S-1}(\theta_{\max}^{(l)} - \theta_{\min}^{(l)}), \quad i = 1, \cdots, S$

  BS simultaneously transmits the FDB beams $\{\mathbf{f}_i^{(l)}\}_{i=1}^{S}$ toward $\{\theta_i^{(l)}\}_{i=1}^{S}$

  $\hat{i}^{(l)} = \arg\max_{i=1,\cdots,S} \left|y_i^{(l)}\right|^2$

  Mobile feeds back the subcarrier index $\hat{i}^{(l)}$ to the BS

end for

$\hat{\phi}_i = \frac{f_i}{f_{\hat{i}(L)}}\left(\theta_{\min}^{(L)} + \frac{\hat{i}(L)-1}{S-1}\left(\theta_{\max}^{(L)} - \theta_{\min}^{(L)}\right)\right), \quad i = 1, \cdots, S$

Output: Subcarrier channel directions $\{\hat{\phi}_i\}_{i=1}^{S}$

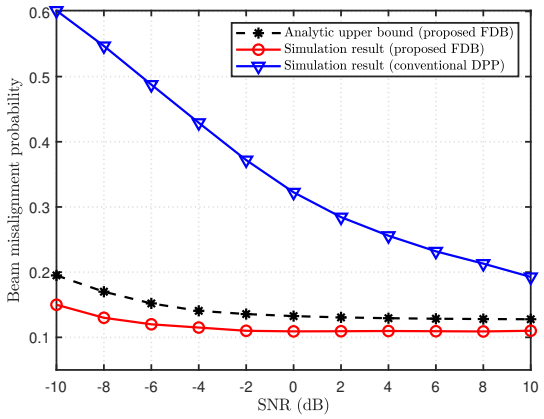

Fig. 8: Beam misalignment probability vs. SNR ($N = 256$, $T = 16$, $P = 16$, and $S = 128$)

where (a) is from the fact that φ is uniformly distributed in $[-\pi, \pi)$. Using the Boole's inequality, P_{miss} can be upper bounded as [23]

$$P_{\text{miss}} \leq \frac{1}{2\pi} \int_{-\pi}^{\pi} \sum_{\hat{i} \neq i^*}^{S} \Pr\big(|y_{i^*}|^2 < |y_{\hat{i}}|^2 \mid \varphi\big) d\varphi. \tag{60}$$

It is worth noticing that $y_i = \sqrt{\rho}\alpha_i \mathbf{a}_N^{\mathrm{H}}\left(\frac{f_i}{f_c}\frac{2\pi d \sin\varphi}{\lambda_c}\right)\mathbf{f}_i + n_i$ is a sum of two independent complex Gaussian random variables $\sqrt{\rho}\alpha_i \mathbf{a}_N^{\mathrm{H}}\left(\frac{f_i}{f_c}\frac{2\pi d \sin\varphi}{\lambda_c}\right)\mathbf{f}_i \sim \mathcal{CN}\left(0, \rho\left|\mathbf{a}_N^{\mathrm{H}}\left(\frac{f_i}{f_c}\frac{2\pi d \sin\varphi}{\lambda_c}\right)\mathbf{f}_i\right|^2\right)$ and $n_i \sim \mathcal{CN}(0, \sigma_n^2)$. Thus, $y_i \sim \mathcal{CN}\left(0, \rho\left|\mathbf{a}_N^{\mathrm{H}}\left(\frac{f_i}{f_c}\frac{2\pi d \sin\varphi}{\lambda_c}\right)\mathbf{f}_i\right|^2 + \sigma_n^2\right)$, which means that $\frac{|y_i|^2}{\rho\left|\mathbf{a}_N^{\mathrm{H}}\left(\frac{f_i}{f_c}\frac{2\pi d \sin\varphi}{\lambda_c}\right)\mathbf{f}_i\right|^2 + \sigma_n^2}$ is a chi-square random variable[6] with degrees of freedom 2.

By denoting $\lambda_i = \frac{|y_i|^2}{\rho\left|\mathbf{a}_N^{\mathrm{H}}\left(\frac{f_i}{f_c}\frac{2\pi d \sin\varphi}{\lambda_c}\right)\mathbf{f}_i\right|^2 + \sigma_n^2} \sim \chi^2(2)$, we obtain the upper bound of P_{miss} as

$$\begin{aligned}
P_{\text{miss}} &\leq \frac{1}{2\pi} \int_{-\pi}^{\pi} \sum_{\hat{i} \neq i^*}^{S} \Pr(|y_{i^*}|^2 < |y_{\hat{i}}|^2 \mid \varphi) d\varphi \\
&= \frac{1}{2\pi} \int_{-\pi}^{\pi} \sum_{\hat{i} \neq i^*}^{S} \Pr\left(\frac{\lambda_{i^*}}{\lambda_{\hat{i}}} < \frac{\rho\left|\mathbf{a}_N^{\mathrm{H}}\left(\frac{f_{\hat{i}}}{f_c}\frac{2\pi d \sin\varphi}{\lambda_c}\right)\mathbf{f}_{\hat{i}}\right|^2 + \sigma_n^2}{\rho\left|\mathbf{a}_N^{\mathrm{H}}\left(\frac{f_{i^*}}{f_c}\frac{2\pi d \sin\varphi}{\lambda_c}\right)\mathbf{f}_{i^*}\right|^2 + \sigma_n^2} \,\middle|\, \varphi\right) d\varphi \\
&\overset{(a)}{=} \frac{1}{2\pi} \int_{-\pi}^{\pi} \sum_{\hat{i} \neq i^*}^{S} F_{\text{cdf}}\left(\frac{\rho\left|\mathbf{a}_N^{\mathrm{H}}\left(\frac{f_{\hat{i}}}{f_c}\frac{2\pi d \sin\varphi}{\lambda_c}\right)\mathbf{f}_{\hat{i}}\right|^2 + \sigma_n^2}{\rho\left|\mathbf{a}_N^{\mathrm{H}}\left(\frac{f_{i^*}}{f_c}\frac{2\pi d \sin\varphi}{\lambda_c}\right)\mathbf{f}_{i^*}\right|^2 + \sigma_n^2}\right) d\varphi \\
&\overset{(b)}{=} \frac{1}{2\pi} \int_{-\pi}^{\pi} \sum_{\hat{i} \neq i^*}^{S} \frac{\rho\left|\mathbf{a}_N^{\mathrm{H}}\left(\frac{f_{\hat{i}}}{f_c}\frac{2\pi d \sin\varphi}{\lambda_c}\right)\mathbf{f}_{\hat{i}}\right|^2 + \sigma_n^2}{\rho\left|\mathbf{a}_N^{\mathrm{H}}\left(\frac{f_{\hat{i}}}{f_c}\frac{2\pi d \sin\varphi}{\lambda_c}\right)\mathbf{f}_{\hat{i}}\right|^2 + \rho\left|\mathbf{a}_N^{\mathrm{H}}\left(\frac{f_{i^*}}{f_c}\frac{2\pi d \sin\varphi}{\lambda_c}\right)\mathbf{f}_{i^*}\right|^2 + 2\sigma_n^2} d\varphi,
\end{aligned} \tag{61}$$

[6]The degree of freedom of $\frac{|y_i|^2}{\rho\left|\mathbf{a}_N^{\mathrm{H}}\left(\frac{f_i}{f_c}\frac{2\pi d \sin\varphi}{\lambda_c}\right)\mathbf{f}_i\right|^2 + \sigma_n^2}$ is 2 since $\mathrm{Re}\{y_i\} \sim \mathcal{N}\left(0, \rho\left|\mathbf{a}_N^{\mathrm{H}}\left(\frac{f_i}{f_c}\frac{2\pi d \sin\varphi}{\lambda_c}\right)\mathbf{f}_i\right|^2 + \sigma_n^2\right)$ and $\mathrm{Im}\{y_i\} \sim \mathcal{N}\left(0, \rho\left|\mathbf{a}_N^{\mathrm{H}}\left(\frac{f_i}{f_c}\frac{2\pi d \sin\varphi}{\lambda_c}\right)\mathbf{f}_i\right|^2 + \sigma_n^2\right)$.

where (a) is from the fact that the ratio $\frac{\lambda_{i^*}}{\lambda_{\hat{i}}}$ of two chi-square random variables λ_i^* and $\lambda_{\hat{i}}$ is an F-distributed random variable and $F_{\text{cdf}}(x) = \Pr(X \leq x)$ is the cumulative distribution function (CDF) of F-distributed random variable X. Also, (b) is from the property that $F_{\text{cdf}}(x) = \frac{x}{x+1}$ [24].

In Fig. 8, we plot the beam misalignment probability as a function of SNR. We observe that the obtained analytic upper bound in (61) is close to the simulation result. We also observe that the beam misalignment probability of FDB is lower than that of the conventional DPP scheme. This is because FDB minimizes the sidelobe leakage of the subcarrier using the intensifier network so that the ratio of RSRPs of the misaligned beam and the optimal beams $\frac{\rho\left|\mathbf{a}_N^{\mathrm{H}}\left(\frac{f_{\hat{i}}}{f_c}\frac{2\pi d\sin\varphi}{\lambda_c}\right)\mathbf{f}_{\hat{i}}\right|^2+\sigma_n^2}{\rho\left|\mathbf{a}_N^{\mathrm{H}}\left(\frac{f_{i^*}}{f_c}\frac{2\pi d\sin\varphi}{\lambda_c}\right)\mathbf{f}_{i^*}\right|^2+\sigma_n^2}$ is much smaller than that of the conventional DPP scheme.

V. Simulation Results

A. Simulation Setup

In this section, we investigate the performance of the proposed FDB. In our simulations, we consider the THz MISO-OFDM systems where the BS equipped with $N = 256$ antennas serves a single-antenna mobile. The mobile is located randomly around the BS within the cell radius of $r = 100\,\text{m}$. We use the wideband THz LoS channel model where the carrier frequency is $f_c = 0.1\,\text{THz}$, the bandwidth is $B = 10\,\text{GHz}$, and the number of subcarriers is $S = 128$. The large-scale fading coefficients are modeled as $\rho = \text{PL} \times 10^{\frac{\sigma_{\text{sh}} z_{\text{sh}}}{10}}$ where PL represents the path loss and $10^{\frac{\sigma_{\text{sh}} z_{\text{sh}}}{10}}$ represents the shadow fading ($\sigma_{\text{sh}} = 4\,\text{dB}$ and $z_{\text{sh}} \sim \mathcal{CN}(0,1)$). We use the path loss model in 3GPP Rel. 16 [25]. The small-scale fading coefficients are generated according to the complex normal distribution (i.e. $\alpha_i \sim \mathcal{CN}(0,1)$). The number of time slots used for the beam management is $L = 5$. We set the transmit SNR to $20\,\text{dB}$. The number of TTDs used in the time delay network and the intensifier network are set to $T = P = \sqrt{N}$. As performance metrics, we use the average data rate defined as $R = \frac{1}{S}\sum_{i=1}^{S}\log_2\left(1+\frac{P_t|\mathbf{h}_i^{\mathrm{H}}\mathbf{f}_i|^2}{\sigma_n^2}\right)$ and the normalized mean square error (NMSE) defined as $\text{NMSE} = 10\log_{10}\left(\frac{1}{S}\sum_{i=1}^{S}\left(\frac{\phi_i-\hat{\phi}_i}{\phi_i}\right)^2\right)$. In each point of the plots, we test at least $100,000$ randomly generated wideband THz systems.

For comparison, we use four benchmark techniques: 1) ideal system with the perfect channel information, 2) DPP-based beam management scheme [18], 3) hierarchical beam management scheme generating the hierarchical beam codebook [11], and 4) 5G NR beam management scheme based on the beam sweeping process [10]. Note, to make a fair comparison between the

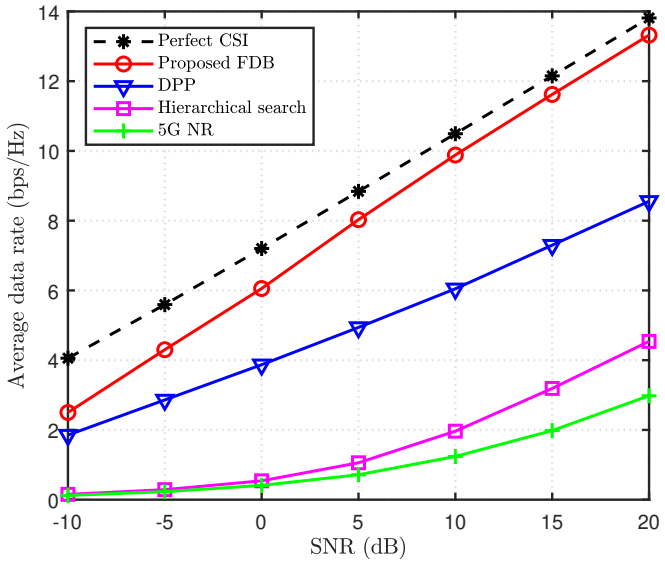

Fig. 9: Average data rate vs. transmit SNR ($N = 256$, $L = 5$, $T = 16$, $P = 16$, and $S = 128$).

DPP and FDB, the number of TTDs used for the DPP beam generation is set to be the same as the total number of TTDs used for the FDB beam generation ($T^{\text{dpp}} = T + P$).

B. Simulation Results

In Fig. 9, we plot the average data rate as a function of the transmit SNR. We observe that FDB outperforms the conventional beam management schemes by a large margin. For example, when SNR $= 10\,$dB, FDB achieves a significant rate gain (more than 670% data rate improvement) over the hierarchical beam management scheme. As mentioned, a phase shift of the conventional schemes relying on the analog phase shifters is invariant to the frequency so the beams for all subcarriers are directed toward the same spatial direction. Since the directions of THz subcarrier channels are distinct due to the beam squint effect (see Section II.A), a mismatch between the analog beam and the subcarrier channels is unavoidable, resulting in a considerable loss of the data rate. Whereas, in the proposed scheme, multiple frequency-dependent beams are generated using the TTD-based phase shifters so that the data rate loss caused by the beam squint effect can be effectively mitigated.

In Fig. 10, we set the transmit SNR to $20\,$dB and plot the NMSE as a function of the number of time slots L. We observe that FDB achieves significant NMSE gains over the conventional schemes. For example, when $L = 5$, FDB achieves more than $30\,$dB and $35\,$dB NMSE gains

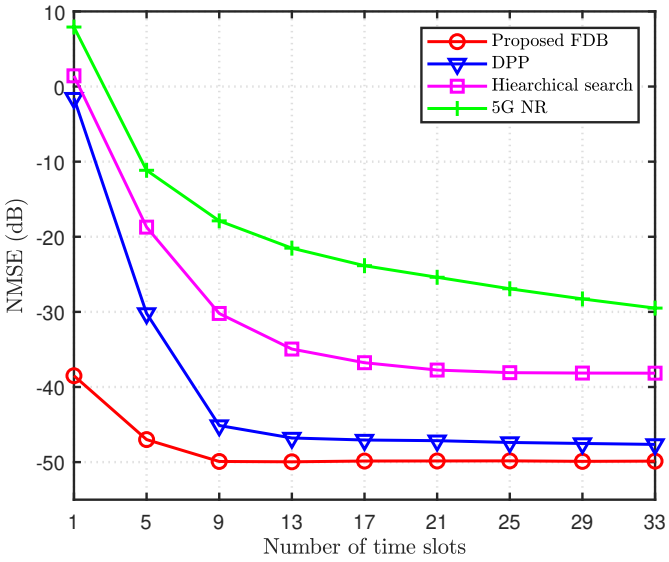

Fig. 10: NMSE vs. the number of time slots ($N = 256$, $T = 16$, $P = 16$, and $S = 128$).

over the hierarchical beam management technique and the 5G NR beam management scheme, respectively. This is not quite a surprise since the conventional schemes search one direction at a time but FDB simultaneously searches $S = 128$ directions. Interestingly, as shown in Fig. 10, FDB can identify pretty accurate beam direction even in a single time slot. Even when compared to DPP, the NMSE gain of the FDB is more than 17 dB since the high sidelobe leakage of DPP will cause a degradation of the beam alignment performance but such is not the case for FDB due to the suppression of the sidelobe leakage using the intensifier network.

In Fig. 11, we plot the average data rate as a function of the number of time slots L. We observe that the proposed scheme achieves more than 70% reduction in the beam management latency over the conventional approaches. For instance, to achieve the average data rate of 13 bps/Hz, FDB requires only $L = 5$ time slots but DPP requires around $L = 17$ time slots. Since FDB can generate very sharp beams achieving the maximum beamforming gain, we also observe that when $L \geq 5$, FDB performs similar to the ideal system with the perfect CSI.

In Fig. 12, we plot the average data rate as a function of the number of transmit antennas N. Interestingly, we observe that the data rate gain of FDB over the conventional schemes increases with the number of antennas. For example, when $N = 64$, FDB shows around 0.6 bps/Hz data rate gain over DPP but it increases up to 6.3 bps/Hz when $N = 400$. This is because when the number of antennas increases, the number of analog phase shifters connected to TTD also

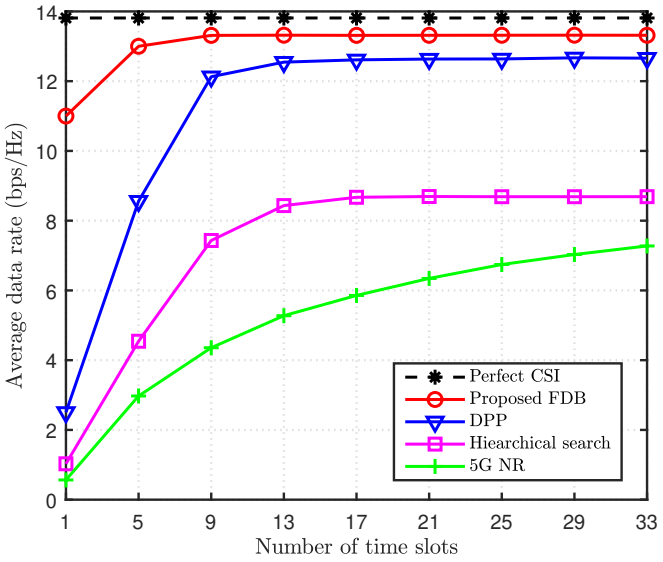

Fig. 11: Average data rate vs. the number of time slots ($N = 256$, $T = 16$, $P = 16$, and $S = 128$).

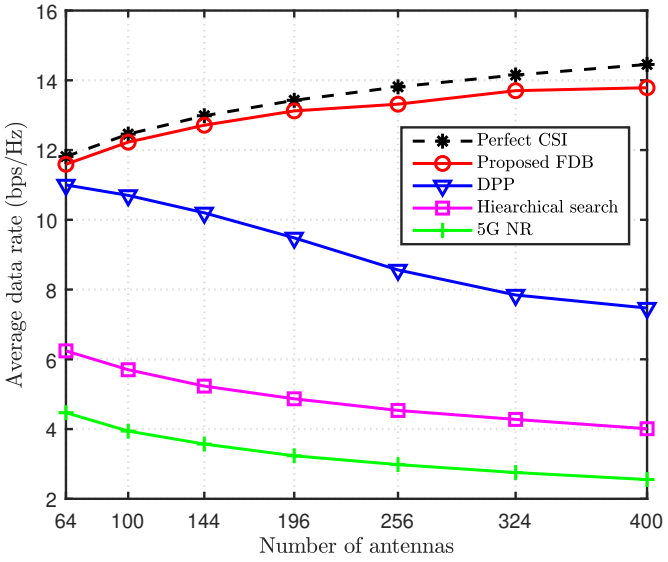

Fig. 12: Average data rate vs. the number of antennas ($L = 5$, $T = \sqrt{N}$, $P = \sqrt{N}$, and $S = 128$).

increases so that the loss of the beamforming gain caused by the mismatch between the DPP beam and the directional beam also increases (see (21)). In contrast, the beamwidth of FDB beams is inversely proportional to the number of antennas so the beam direction accuracy increases with

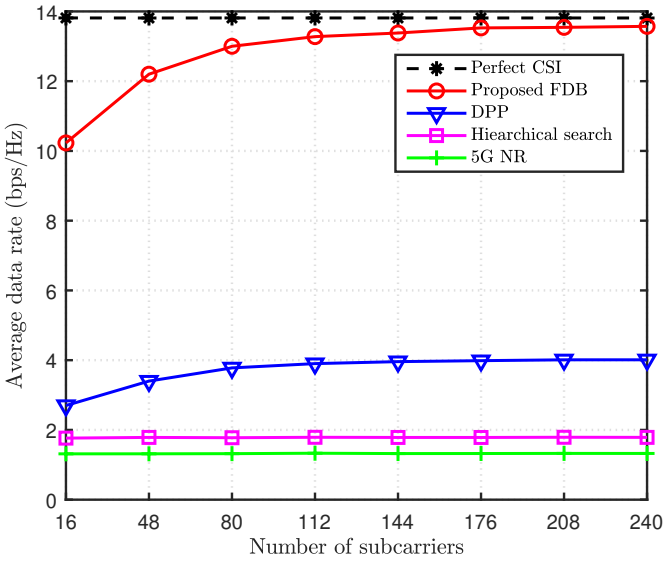

Fig. 13: Average data rate vs. the number of subcarriers ($N = 256$, $L = 2$, $T = 16$, and $P = 16$).

the number of antennas. This implies that FDB would be more effective in the THz ultra-massive MIMO systems where the number of antennas is extremely large.

In Fig. 13, we set the number of time slots to $L = 2$ and plot the average data rate as a function of the number of subcarriers S. We observe that the performance gain of FDB increases with the number of subcarriers. Specifically, when the number of subcarriers increases from $S = 16$ to $S = 240$, the data rate gain of FDB over the conventional DPP-based scheme increases from 7.5 bps/Hz to 9.6 bps/Hz. This is because FDB hierarchically finds out the beam direction so that the beam direction accuracy increases exponentially with the number of subcarrier beams. Whereas, DPP uniformly splits the probing area and then sequentially searches the divided areas so that the beam direction accuracy increases linearly with the number of subcarrier beams.

VI. Conclusion

In this paper, we proposed a THz beam management scheme that simultaneously generates multiple frequency-dependent beams using the TTD-based phase shifters. By employing the generated FDB beams as the training beams, the proposed technique searches multiple directions (as many as the number of subcarriers) simultaneously, thereby reducing the beam management latency. Intriguing feature of the proposed FDB is to exploit a deliberately designed TTD-based

signal propagation network called intensifier to bridge the gap between the desired beamforming vectors and the frequency-dependent beamforming vectors. In doing so, RSRP of the beam aligned with the channel propagation path gets larger while those of the misaligned beams get smaller, resulting in the significant improvement of the beam direction accuracy. From the beam misalignment probability analysis and the numerical evaluations on 6G THz environment, we demonstrated that FDB is very effective in improving the beam direction accuracy and also reducing the beam management latency. In our work, we restricted our attention to THz communications, but there are many interesting applications of FDB including vehicle-to-everything (V2X) communications and reconfigurable intelligent surface (RIS)-assisted communications.

APPENDIX

A. *Proof of Lemma 2*

First, the channel direction $\phi_{\hat{i}^{(0)}}$ of the $\hat{i}^{(0)}$-th subcarrier channel is upper bounded as

$$\phi_{\hat{i}^{(0)}} - \theta_{\hat{i}^{(0)}} \leq \theta_{\hat{i}^{(0)}+1} - \phi_{\hat{i}^{(0)}+1}. \tag{62}$$

Recalling that $\phi_{\hat{i}^{(0)}} = \frac{f_{\hat{i}^{(0)}}}{f_c}\pi \sin\varphi$ (see (4)), the upper bound of $\sin\varphi$ is

$$\pi \sin\varphi \leq \frac{(\theta_{\hat{i}^{(0)}} + \theta_{\hat{i}^{(0)}+1})f_c}{(f_{\hat{i}^{(0)}} + f_{\hat{i}^{(0)}+1})}. \tag{63}$$

Similarly, the lower bound of $\sin\varphi$ is

$$\pi \sin\varphi \geq \frac{(\theta_{\hat{i}^{(0)}} + \theta_{\hat{i}^{(0)}-1})f_c}{(f_{\hat{i}^{(0)}} + f_{\hat{i}^{(0)}-1})}. \tag{64}$$

Combining (63) and (64), $\sin\varphi$ is bounded as

$$\frac{(\theta_{\hat{i}^{(0)}} + \theta_{\hat{i}^{(0)}-1})f_c}{(f_{\hat{i}^{(0)}} + f_{\hat{i}^{(0)}-1})} \leq \pi \sin\varphi \leq \frac{(\theta_{\hat{i}^{(0)}} + \theta_{\hat{i}^{(0)}+1})f_c}{(f_{\hat{i}^{(0)}} + f_{\hat{i}^{(0)}+1})}. \tag{65}$$

Finally, using $\phi_i = \frac{f_i}{f_c}\pi \sin\varphi$, we obtain the bound of the subcarrier channel directions $\{\phi_i\}_{i=1}^{S}$ as

$$\frac{\left(\theta^{(0)}_{\hat{i}^{(0)}} + \theta^{(0)}_{\hat{i}^{(0)}-1}\right)f_i}{f_{\hat{i}^{(0)}} + f_{\hat{i}^{(0)}-1}} \leq \phi_i \leq \frac{\left(\theta^{(0)}_{\hat{i}^{(0)}} + \theta^{(0)}_{\hat{i}^{(0)}+1}\right)f_i}{f_{\hat{i}^{(0)}} + f_{\hat{i}^{(0)}+1}}, \quad i = 1, \cdots, S. \tag{66}$$

REFERENCES

[1] Z. Zhang, Y. Xiao, Z. Ma, M. Xiao, Z. Ding, X. Lei, G. K. Karagiannidis, and P. Fan, "6G wireless networks: Vision, requirements, architecture, and key technologies," *IEEE Veh. Technol. Mag.*, vol. 14, no. 3, pp. 28–41, 2019.

[2] M. Giordani, M. Polese, M. Mezzavilla, S. Rangan, and M. Zorzi, "Toward 6G networks: Use cases and technologies," *IEEE Commun. Mag.*, vol. 58, no. 3, pp. 55–61, 2020.

[3] I. F. Akyildiz, C. Han, Z. Hu, S. Nie, and J. M. Jornet, "Terahertz band communication: An old problem revisited and research directions for the next decade," *IEEE Trans. Commun.*, vol. 70, no. 6, pp. 4250–4285, 2022.

[4] I. F. Akyildiz, J. M. Jornet, and C. Han, "TeraNets: Ultra-broadband communication networks in the terahertz band," *IEEE Wirel. Commun.*, vol. 21, no. 4, pp. 130–135, 2014.

[5] C. Han and Y. Chen, "Propagation modeling for wireless communications in the terahertz band," *IEEE Commun. Mag.*, vol. 56, no. 6, pp. 96–101, 2018.

[6] H. Ji, Y. Kim, J. Lee, E. Onggosanusi, Y. Nam, J. Zhang, B. Lee, and B. Shim, "Overview of full-dimension MIMO in LTE-advanced pro," *IEEE Commun. Mag.*, vol. 55, no. 2, pp. 176–184, 2016.

[7] S. Kim, J. W. Choi, and B. Shim, "Downlink pilot precoding and compressed channel feedback for FDD-based cell-free systems," *IEEE Trans. Wirel. Commun.*, vol. 19, no. 6, pp. 3658–3672, 2020.

[8] Y.-N. R. Li, B. Gao, X. Zhang, and K. Huang, "Beam management in millimeter-wave communications for 5G and beyond," *IEEE Access*, vol. 8, pp. 13 282–13 293, 2020.

[9] Y. Ahn, J. Kim, S. Kim, K. Shim, J. Kim, S. Kim, and B. Shim, "Towards intelligent millimeter and terahertz communication for 6G: Computer vision-aided beamforming," *IEEE Wireless Commun.*, 2022.

[10] M. Giordani, M. Polese, A. Roy, D. Castor, and M. Zorzi, "A tutorial on beam management for 3GPP NR at mmWave frequencies," *IEEE Commun. Surv. Tuts.*, vol. 21, no. 1, pp. 173–196, 2018.

[11] Z. Xiao, T. He, P. Xia, and X.-G. Xia, "Hierarchical codebook design for beamforming training in millimeter-wave communication," *IEEE Trans. Wirel. Commun.*, vol. 15, no. 5, pp. 3380–3392, 2016.

[12] C. Lin, G. Y. Li, and L. Wang, "Subarray-based coordinated beamforming training for mmWave and sub-THz communications," *IEEE J. Sel. Areas Commun.*, vol. 35, no. 9, pp. 2115–2126, 2017.

[13] R. Zhang, H. Zhang, W. Xu, and X. You, "Subarray-based simultaneous beam training for multiuser mmWave massive MIMO systems," *IEEE Wirel. Commun. Lett.*, vol. 8, no. 4, pp. 976–979, 2019.

[14] H. Echigo, Y. Cao, M. Bouazizi, and T. Ohtsuki, "A deep learning-based low overhead beam selection in mmWave communications," *IEEE Trans. Veh. Technol.*, vol. 70, no. 1, pp. 682–691, 2021.

[15] R. Rotman, M. Tur, and L. Yaron, "True time delay in phased arrays," *Proc. IEEE*, vol. 104, no. 3, pp. 504–518, 2016.

[16] B. Zhai, A. Tang, C. Peng, and X. Wang, "SS-OFDMA: Spatial-spread orthogonal frequency division multiple access for terahertz networks," *IEEE J. Sel. Areas Commun.*, vol. 39, no. 6, pp. 1678–1692, 2021.

[17] H. Hashemi, T.-S. Chu, and J. Roderick, "Integrated true-time-delay-based ultra-wideband array processing," *IEEE Commun. Mag.*, vol. 46, no. 9, pp. 162–172, 2008.

[18] J. Tan and L. Dai, "Wideband beam tracking in THz massive MIMO systems," *IEEE J. Sel. Areas Commun.*, vol. 39, no. 6, pp. 1693–1710, 2021.

[19] 3GPP, "Study on New Radio (NR) Access Technology - Physical Layer Aspects - Release 14," 3rd Generation Partnership Project (3GPP), TR 38.802, 2017.

[20] A. Faisal, H. Sarieddeen, H. Dahrouj, T. Y. Al-Naffouri, and M.-S. Alouini, "Ultramassive MIMO systems at terahertz bands: Prospects and challenges," *IEEE Veh. Technol. Mag.*, vol. 15, no. 4, pp. 33–42, 2020.

[21] B. Wang, M. Jian, F. Gao, G. Y. Li, and H. Lin, "Beam squint and channel estimation for wideband mmWave massive MIMO-OFDM systems," *IEEE Trans. Sig. Process.*, vol. 67, no. 23, pp. 5893–5908, 2019.

[22] L. Dai, J. Tan, Z. Chen, and H. V. Poor, "Delay-phase precoding for wideband THz massive MIMO," *IEEE Trans. Wireless Commun.*, 2022.

[23] P. Diananda and M. Bartlett, "Some probability limit theorems with statistical applications," in *Proc. Cambridge Philos. Soc.*, vol. 49, no. 2. Cambridge University Press, 1953, pp. 239–246.

[24] W. Wells, R. Anderson, and J. W. Cell, "The distribution of the product of two central or non-central chi-square variates," *Ann. Math. Statist.*, vol. 33, no. 3, pp. 1016–1020, 1962.

[25] "Study on channel model for frequencies from 0.5 to 100 GHz," *3GPP TR, 38.901, V16.1.0*, 2020.

Abstract (In Korean)

테라헤르츠 통신은 더 풍부한 스펙트럼 자원을 확보하고 대역폭 사막을 극복할 수 있는 매력적인 방법으로 간주된다. 테라헤르츠 통신의 주요 어려움 중 하나는 높은 회절 및 침투 손실과 대기 흡수로 인한 신호 전력의 심각한 감쇠다. 이러한 심각한 경로 손실을 보상하기 위해 대규모 MIMO(multiple-input multiple-output)로 구현한 빔 형성 기법이 널리 사용되고 있다. 빔 형성 이득은 빔이 신호 전파 경로에 적절하게 정렬되어야만 최대화되므로 정확한 빔 방향 획득이 매우 중요하다. 기존의 빔 관리 방식의 주요 문제는 훈련 빔의 수에 비례하는 상당한 대기 시간이다. 본 논문에서는 TTD(True Time Delay) 기반 위상 천이기를 이용하여 다중 주파수 종속 빔을 동시에 생성하는 테라헤르츠 빔 관리 기법을 제안한다. Intensifier라고 하는 TTD 기반 신호 전파 네트워크를 사용하여 주파수 종속 빔 형성 벡터와 원하는 방향성 빔 형성 벡터 사이의 간격을 좁힘으로써 빔 형성 이득을 최대화하는 매우 날카로운 훈련 빔을 생성한다. 수치 결과로부터 제안된 방식이 빔 관리 대기 시간을 70% 이상 감소시키고 데이터 속도를 60% 증가시키는 것을 보였다.

핵심어: 테라헤르츠 통신, 대규모 MIMO, 빔 관리